Resiliency-Driven Multi-Step Critical Load Restoration Strategy Integrating On-Call Electric Vehicle Fleet Management Services

Ayşe Kübra Erenoğlu, *Graduate Student Member, IEEE*, Semanur Sancar, *Student Member*, *IEEE*, İdil Su Terzi, Ozan Erdinç, *Senior Member, IEEE,* Miadreza Shafie-khah*, Senior Member, IEEE*, and João P. S. Catalão*, Fellow, IEEE*

***Abstract*—In order to enhance the restoration capability of the distribution system during emergency conditions, a resiliency-driven critical load restoration strategy is propounded in this paper. Electric vehicles (EVs) are considered for the grid-support services to deal with challenges on such occasions, in order to maintain the power supply continuity of critical loads by reducing the number of outage periods. The collaboration between fleet operator and distribution system operator is considered in the proposed scheme, making it possible to direct available EVs to the damaged areas. The random characteristic of the seismic event is captured by generating numerous hazard scenarios using a probabilistic approach with the Monte Carlo Simulation (MCS) technique. Afterwards, the unavailability of overhead distribution branches is determined within the fragility curve concept. Besides, the uncertainties caused by EV mobility are considered by performing learning-based analyses for forecasting the location and amount of EVs in the related zone. The obtained data is processed as input parameters in a mixed-integer linear programming (MILP) framework-based stochastic model. Besides, the conceptually developed interfaces for all stakeholders in the proposed scheme are described in detail for bridging the gap between the theoretical background of the concept and practical real-world implementation.**

***Index Terms*—Electric vehicles, forecasting, mixed-integer linear programming, optimization, resiliency, restoration strategy.**

NOMENCLATURE

A. Sets and Indices

Ω_i^f	Subset of substation buses.
$d \in D$	Set of load types.
$e \in E$	Set of electric vehicles.
$i \in I$	Set of buses.
$i' \in I$	Subset of buses.
$l \in L$	Set of branches.
$p \in P$	Set of points.
$t \in T$	Set of time periods.
$s \in S$	Set of damaged locations.
$v \in V$	Set of extreme event occurrence time.

B. Parameters

$\delta_{d,t}$	Rated power demand of load type d during period t [kW].
η_e	Discharging efficiency of EV e.
κ_i	Socket number of bus i.
$b_{i,e}$	Binary parameter; 1 if EV e is available for bus i during an event, else 0.
DR_e	Discharging rate of EV e [kW].
f_l^{max}	Power flow capacity of branch l [kW].
$h_{i,d}$	Binary parameter: 1 if load d exists in bus i, else 0.
$P_i^{f,max}$	Maximum power injection capacity of substation bus [kW].
$soe_{e,t}$	State-of-energy of EV e at t_{event} [kWh].
soe_e^{loss}	State-of-energy losses of EV e [kWh].
SOE_{min}	Minimum state-of-energy level of EV [kWh].
$t_{arrival}$	Arrival time of EV.
$t_{departure}$	Departure time of EV.
t_{event}	Event time.
Y_p	The y coordinate point of point p.
X_p	The x coordinate point of point p.
ε	Very small number.

C. Variables

$\alpha_{i,e,s,v,t}$	Binary variable: 1 if EV e is connected to candidate bus during period t in scenario s and v, else 0.
$\beta_{i,e,s,v,t}$	Binary variable; 1 if $\alpha_{i,e,t}$ is 0 in scenario s and v, else 0.
$F_{l,s,v,t}$	Square of the flow through branch l during period t in scenario s and v [kW^2].
$f_{l,s,v,t}$	Active power flow of branch l during period t in scenario s and v [kW].
$P_{i,e,s,v,t}^{dis}$	Discharge power of EV e at bus i during period t in in scenario s and v [kW].
$P_{i,s,v,t}^{f}$	Total active power provided by substation at bus i during period t in scenario s and v [kW].
$P_{i,s,v,t}^{fleet}$	Total discharge power of EVs connected to bus i during period t in scenario s and v [kW].
$P_{i,s,v,t}^{f,load}$	Active power provided by substation at bus i during period t to cover the related demand in scenario s and v [kW].
$P_{i,s,v,t}^{demand}$	Total power demand at bus i during period t in scenario s and v [kW].
$P_{l,s,v,t}^{loss}$	Power losses of branch l during period t in scenario s and v [kW].
$SOE_{i,e,s,v,t}$	State-of-energy of EV e at period t in scenario s and v [kWh].
$u_{i,s,v,t}^{d}$	Binary variable: 1 if the load d is fed by bus i in scenario s and v, else 0.
$z_{l,s,v,t,p}$	SOS2 variable for linearization.

The work of J.P.S. Catalão was supported in part by FEDER funds through COMPETE 2020 and in part by the Portuguese funds through FCT under POCI-010145-FEDER-029803 (02/SAICT/2017). (*Corresponding authors: M. Shafie-khah; J.P.S. Catalão*).

A.K. Erenoğlu, S. Sancar, İ.S. Terzi, and O. Erdinç are with the Department of Electrical Engineering, Yildiz Technical University, 34349 Istanbul, Turkey (e-mails: ayseerenoglu94@gmail.com; semanursancarytu@gmail.com; idilsuterziytu@gmail.com; oerdinc@yildiz.edu.tr).

M. Shafie-khah is with the School of Technology and Innovations, University of Vaasa, 65200 Vaasa, Finland (e-mail: mshafiek@univaasa.fi).

J.P.S. Catalão is with the Faculty of Engineering of University of Porto, and INESC TEC, Porto, Portugal (e-mail: catalao@fe.up.pt).

I. INTRODUCTION

Power system is one of the most critical infrastructures that need to be hedged against threats for ensuring resilient and secure operation in our modern era. However, the highly infrequent events such as earthquakes, hurricanes and floods have significant impacts on power grid which bring great amount of losses also with putting millions of end-users into darkness. Transmission towers, switchyards and overhead lines are particularly vulnerable places which may be partially or fully damaged due primarily to earthquakes [1]. As an example, end-users suffered from power outages in Texas for approximately 14 days due to Hurricane Harvey [2].

Furthermore, the increased probability of wide-area electrical blackouts provoked by HILP (high impact-low probable) events has been expected to increase in today's world as a direct impact of global warming [3]. Hence, combatting with rare but destructive events is a major task for utility decision-makers from the concept of resiliency. In order to boost power grid resiliency in emergency conditions, broad number of smart solutions have been considered to deal with potential consequences in the literature.

Distributed energy resources consisting of distributed generation (DG), energy storage systems (ESSs) and demand response (DR) strategies, microgrid (MG) architectures and electric vehicles (EVs) are the most promising approaches that contribute to improve optimal hardening strategies in such HILP occasions. Deploying modular DG resources, ESSs and MGs have been employed for maintaining the power supply continuity to local end-users; however, they are in fixed areas and serve local loads in restricted islanded places, but surely not further-away. On the other hand, mobile sources can serve prioritized critical loads with creating multiple islands within the network. The concept of utilizing EVs and other mobile power sources in service restoration strategies have been shown great interest. Sun et al. [4] developed a MILP-based bottom-up system restoration plan for utilizing the capabilities of hybrid EVs to recover entire system with maximizing restored energy. In [5], routing and scheduling of EVs were taken under study for utilizing their storage capacities in serving critical loads during emergencies as well as taking the advantage of price arbitrage opportunities for EV owners.

Rahimi and Davoudi et al. [6] presented an investigation whether utilizing hybrid and battery EVs in vehicle-to-home (V2H) mode of operation would be a feasible solution or not in terms of increasing resiliency during widespread damage occurrence in distribution system side in a hurricane event. Similarly, the study in [7] proposed a home energy management framework with managing EVs in V2H mode for the purpose of increasing self-healing capability in case of any failure. Shin et al. [8] proposed a novel algorithm for optimizing V2H operation with the objective of minimizing load curtailment of residential end-users in islanded mode when a grid failure occurs.

In order to pre-position and route mobile energy generators in real-time for recovering critical loads in case of a natural disaster by forming multiple MGs, the study in [9] proposed a two-stage dispatch framework with also considering traffic issues. Yang et al. [10] proposed a two-stage distribution system restoration framework in which optimal routing and scheduling of mobile power sources consisting of mobile emergency generators, mobile ESSs and EVs also coordinating with distribution system dynamic network reconfiguration were performed to increase critical load restoration. Gao et al. [11] focused on the resource allocation problem of distribution system which mainly aimed to supply critical loads in post-hurricane restoration periods with deploying diesel oil, electric buses and transportable batteries. However, the installation of large-scale mobile ESSs with great amount of capacity requires higher installation and maintenance costs.

In order to dispatch mobile power sources and repair crews in the transportation system after a major outage to maximize the cumulated service time to critical loads, a MILP-based critical load restoration problem was developed in [12]. The dynamic traffic state and traffic congestion were considered after an event. Similarly, Lei et al. [13] formulated the co-optimization problem of distribution restoration with dispatching and routing the repair crews and mobile power sources in the transportation network to increase resiliency. The work proposed in [14] aimed to utilize mobile energy generators in reliability enhancement strategies in case of unintentional islanding and unplanned outages occurring in MG. The study presented in [15] aimed to take advantages of mobile ESSs in resiliency enhancement strategies of power distribution system for both performing an economical decision in investment and emergency operational phases. The consequences of unintentional islanding due to natural disasters were aimed to be mitigated in [16] with optimal scheduling of emergency resources which were DR strategies, ESS, DERs as well as minimizing the expected social cost. From the similar point of view, EVs, DGs, DR implementations, ESS were considered in [17] as supplemental resources for minimizing load shedding of critical-loads in islanded mode of operation of an MG.

Even though many more studies provided contributions in the field of using EV as a mobile supplemental resource, it is to be highlighted that the availability conditions of EVs was neglected in the presented studies [4]-[8], [10]-[11], [15]. On the other hand, the models devised in [4]-[9], [12]-[15] ignored the stochasticity regarding the damaged location based on the seismic intensity characterization, while the studies presented in [4]-[9], [11]-[17] did not consider the developing interfaces for communication. This study has some important differences from the existing literature, especially considering the stochasticity handling method, optimal power flow and objective function, determining the availability conditions of EVs together with developing user-friendly interfaces. The major contributions of the study are as follows:

- In order to characterize the inherent uncertainties due primarily to EV mobility and to determine the input parameters of the optimization algorithm in an accurate and reasonable fashion, learning-based analyses are performed in the first step. The real yearly data of yellow taxis is used to forecast the available V2G capacity for enabling efficient and realistic operational strategies.
- The stochasticity regarding the event occurrence time and damaged location is handled by a scenario-based stochastic approach for capturing the dynamic characteristics of the uncertainties. The potential scenarios are created based on the seismic intensity characterization by calculating the peak ground acceleration (PGA) in the location of interest, due to the attenuation relationship (AR) with generating a high amount of earthquake scenarios via the Monte Carlo Simulation (MCS) method. Afterwards, the failure probability of overhead branches is determined within the fragility curve concept.
- A user-friendly interface platform that does not require an advanced communication infrastructure is developed in the scope of the study considering possible disruptions on the existing communication system. The proposed interface does not have a theoretical contribution but has an applicability-oriented contribution to the possible real-world consideration of the theoretical concept. The relevant industry will need such easy-to-use interfaces for non-experts end-users in order to obtain more effective performance for such strategies.

The organization of the article as follows: Section II describes the learning-based analyses for EV dispatch together with seismic intensity characterization and developed interfaces for each stakeholder. MILP-based mathematical formulation for critical load restoration concept is described in Section III. The numerical results are discussed on the IEEE-33 bus test systems in Section IV. Concluding remarks are presented in Section V.

II. Methodology

In the proposed system, it is assumed that there are critical and non-critical loads connected to several low voltage buses in the distribution system that should be supplied by the feeder and EVs during normal and emergency conditions, respectively. When disruptions occur in any part of the network due to an extreme event, EVs under the fleet operator framework are considered as grid-support services with operating ability of V2G mode. In order to prevent prolonged outages, EVs play a vital role in service restoration processes by travelling from the staging locations to damaged areas. The optimal load restoration strategy is performed thanks to the effective cooperation with fleet operator and distribution system operator with two-way information flow. The fleet operator has responsibility to determine availability matrices of EVs with extracting the location, battery SoE levels, minimum and maximum SoE and maximum discharging rate of EVs via the developed interface.

On the other hand, the distribution system operator sends a signal to fleet operator from cloud to server for announcing damaged locations, possible connection points and their socket numbers for picking up critical loads during an emergency condition. The related data transfers from main server to the fleet operator. Also, the fleet operator interface is designed via the object-oriented development method Python pyqt5 and Kivy frameworks. The general framework of proposed concept is illustrated in Fig. 1.

A. Assessment of Seismic Intensity

The overall framework of the post-event resiliency-driven strategy consisting of three main stages is demonstrated in Fig. 2. In the first stage, PGA used in defining ground shaking at the location of overhead distribution branches is estimated. PGA is a very important ground motion parameter, and it can be determined by AR in the literature [18]. To model the attenuation of released seismic energy of an earthquake at the location of interest, several factors should be determined as an initial step. The geological and topographical effects of the site, source specification, the properties of the soil and sediments, fault type, seismic potential of the faults, potential earthquake magnitudes as well as the distance from the hypocenter are processed in algorithmic procedures to obtain probabilistic derivations of AR [19].

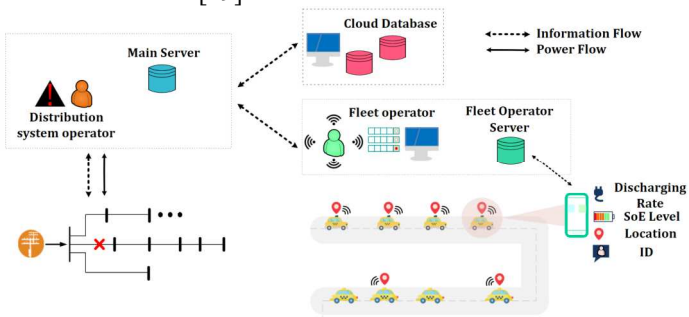

Fig. 1. Proposed critical load restoration framework.

A general analytical formulation to quantify AR is following according to the [20]:

$$\ln(\phi) = \omega + f(M) + f(R) + f(Z) + \varepsilon \quad (1)$$

The random characteristics of the seismic event are the major challenge [21] for the system operators while they are preparing a management strategy. Since the earthquake dynamics cannot be estimated accurately, generating a great number of hazard scenarios using a probabilistic approach with the MCS technique becomes a promising solution in this manner. Considering the stochastic nature of a seismic event in terms of bringing about uncertainties in both spatial and temporal aspects, the distribution system of interest is divided into several zones in this study. After, 100,000 earthquake scenarios are created based on the ground motion parameters such as moment magnitude, hypocenter distance and soil type of the studied area.

Accordingly, the damage level of overhead distribution branches is determined in the concept of fragility curve which represents the relationship between the failure probability of the specific component and seismic intensity (e.g., PGA) [22]. To assess the availability and/or unavailability of distribution line sections in the network, five damage states are introduced considering that not all branches have the same response to the extreme shocks as shown in Fig. 3 [23]. Complete damage, extensive, moderate, slight, and none are defined as among the inputs contributing to the optimization-based restoration strategy. According to [24], each fragility curve is described by a median value of the PGA parameter and log-normal standard deviation (β) corresponding to the damage state thresholds and their variability. The probability of being in or exceeding a damaged state is modeled as a cumulative lognormal distribution as follows:

$$P[\zeta|S_d] = \varphi[\frac{1}{\beta_\zeta}\ln(\frac{S_d}{\overline{S_{d,\zeta}}})] \quad (2)$$

Herein, spectral displacement and its median value are indicated as S_d and $\overline{S_{d,\zeta}}$, respectively. Also, β_ζ states the standard deviation of the natural logarithm of spectral displacement for damage state, ζ, and φ is the standard normal cumulative distribution function.

Integration of fragility curves is pursued in this study to diagnose the status of distribution branches when subjected to an extreme seismic event. The individual failure probability of each of five states (as indicated above) of damage is calculated corresponding to being exposed PGA parameter as follows:

$$P_{Nn} = 1 - P[Nn|\gamma] \quad (3)$$

$$P_S = P[S|\gamma] - P[Ex|\gamma] \quad (4)$$

$$P_{Md} = P[Md|\gamma] - P[Ex|\gamma] \quad (5)$$

$$P_{Ex} = P[Ex|\gamma] - P[Cm|\gamma] \quad (6)$$

Herein, Cm, Ex, Md, S, Nn indicate the damage status of the electrical component of interest as complete, extensive, moderate, slight, none, respectively. After calculating each damage state probability, the state of the overhead distribution line section is obtained from the following equations.

$$L^{total} = \sum_n length_n \quad (7)$$

$$v_n^{ls} = \frac{length_n}{L^{total}} \times [P_S F_S + P_{Md} F_{Md} + P_{Ex} F_{Ex} + P_{Cm} F_{Cm}] \quad (8)$$

This article has been accepted for publication in a future issue of this journal, but has not been fully edited. Content may change prior to final publication. Citation information: DOI 10.1109/TSG.2022.3155438, IEEE Transactions on Smart Grid

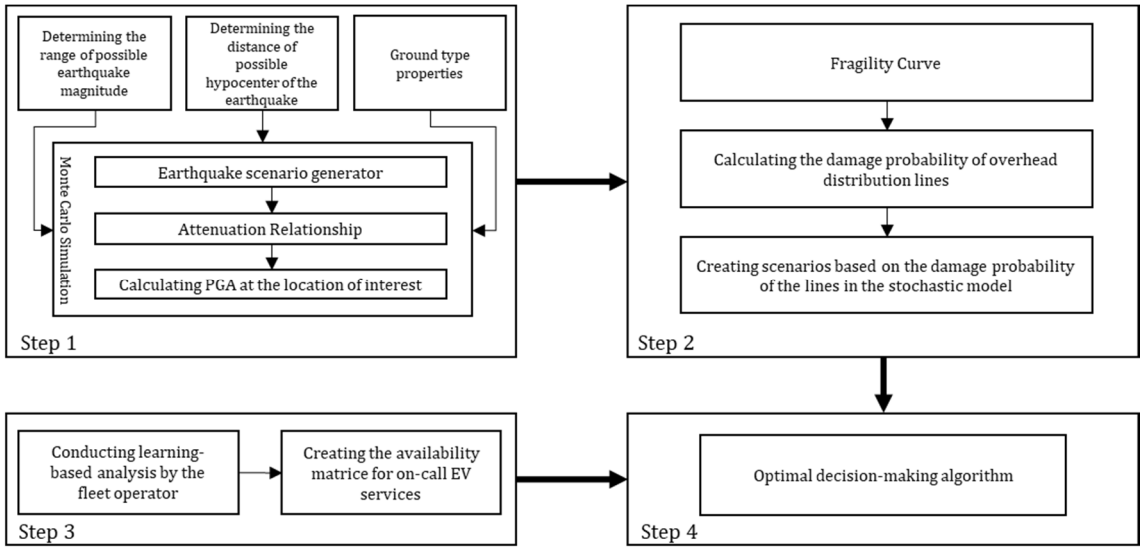

Fig. 2. Big picture of the proposed multi-step optimal decision-making model.

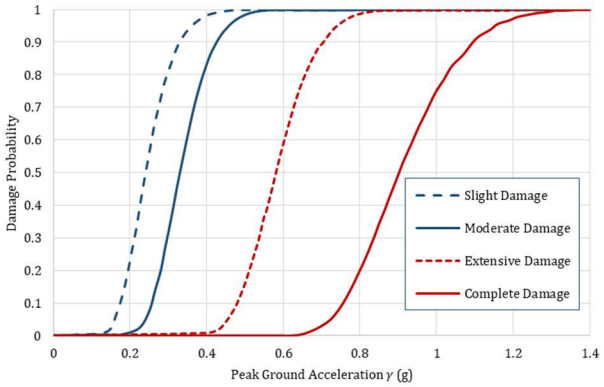

Fig. 3. Fragility curve of the overhead distribution branches [23].

where v_n^{ls} denotes the unavaliability of line section n when exposed to direct effect of a seismic shock. On the other hand, F_{Cm}, F_{Ex}, F_{Md}, F_S indicates the failure of 80%, 50%, 12% and 4% of all distribution branches [24].

B. Learning-based Analyses for EV Dispatch in Response to Extreme Event

The uncertainties caused by EV mobility bring significant problems for providing grid-support services in case of large-scale outages. In order to capture this impact and create more accurate availability matrices, forecasting systems are presented as realistic and cost-effective strategies in determining location and the amount of EVs in any zone. Time series-based historical data of yellow taxis between 01/11/2018 to 01/12/2019, obtained from the New York City Taxi and Limousine Commission (TLC) website [25] in minute scale, is used in this study. Two neighborhoods in Manhattan which are Alphabet City and Two Bridges/Seward Park are selected for forecasting the number of yellow taxis and their locations in case of large-scale failure at nearby damaged zones for IEEE-33 bus test system. A flow chart given in Fig. 4 helps to understand the overall operation of learning-based analysis in better way.

PROPHET developed by Facebook Core Data Science Team which is an open-source software and available for Python is popular in terms of forecasting time series data where non-linear trends are fit with daily seasonality including holiday effects, weekly and annually [26].

PROPHET uses a decomposable time series model consisting of three fundamental components: trend, seasonality, and holidays which are also indicated by [27]: $y(t) = g(t) + s(t) + h(t) + \in_t$. The algorithm is durable to missing data, capable of capturing shifts in the trend as well as handling large outliers. It makes possible to obtain reasonable estimations of mixed data without spending manual effort and presents an environment for predicting desired values with high quality but in an easy way [28].

C. Developed Interface

In this subsection, the conceptually developed interfaces considering simultaneously the key players such as the EV users, fleet operator and distribution system operator are presented comprehensively. The major motivation of the proposed architecture is to facilitate the participation of EV users in the emergency response actions and to improve grid post-event restoration capability. Collaborated operation between mentioned stakeholders creates a notable ecosystem in which bi-directional information exchange is provided by the main server through an internet connection. To describe the operation procedure of the proposed framework in a better way, Fig. 5 is illustrated including the main steps of the concept. It should be underlined that smartphones are preferred rather than specific commercial devices for keeping in touch with the end-users in the platform. While considering the impacts of extreme events on the communication infrastructure, mobile phone-based applications can be probably evaluated as one of the most effective and economic ways to tackle the challenges in terms of implementing the theoretical background of the study to the real-world application.

The proposed interface is shown in Fig. 6 (a) and (b) is created as a web-based application in Google COLAB platform for distribution system operator and then converted to mobile-based application in Python Kivy framework. As can be seen in the related figure that the system operator can monitor the whole network status such as connections and disconnections of the loads. Damaged overhead lines are marked in red while those which remain in operation are marked in green.

The system operator conveys the need for grid-support resources to the fleet operator via the internet by sharing information about the network.

This article has been accepted for publication in a future issue of this journal, but has not been fully edited. Content may change prior to final publication. Citation information: DOI 10.1109/TSG.2022.3155438, IEEE Transactions on Smart Grid

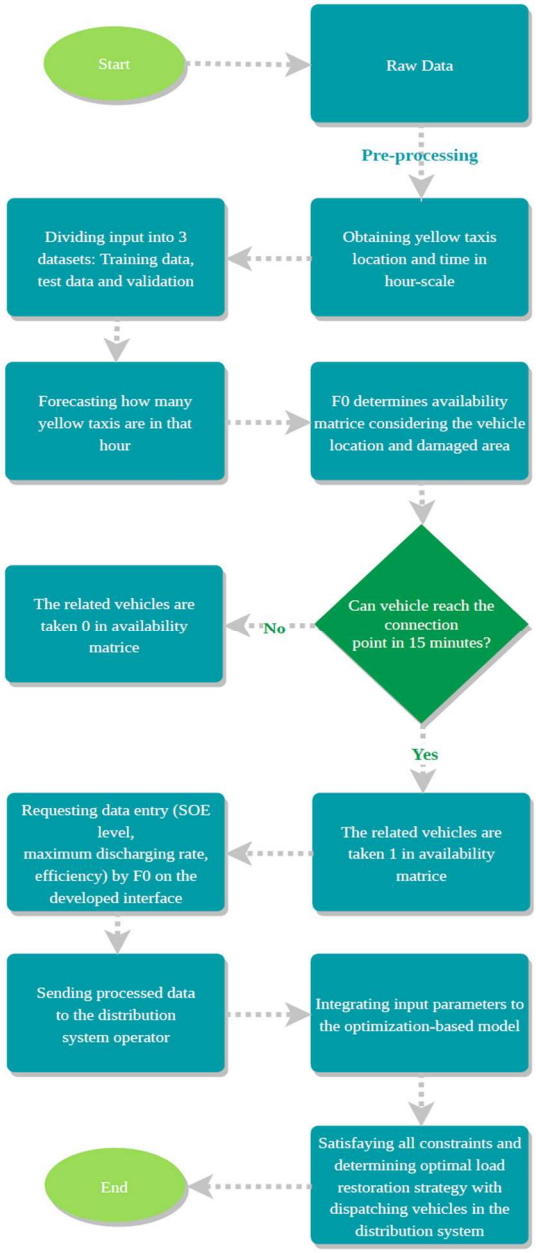

Fig. 4. Flow chart of the overall operation of multi-step critical load restoration strategy.

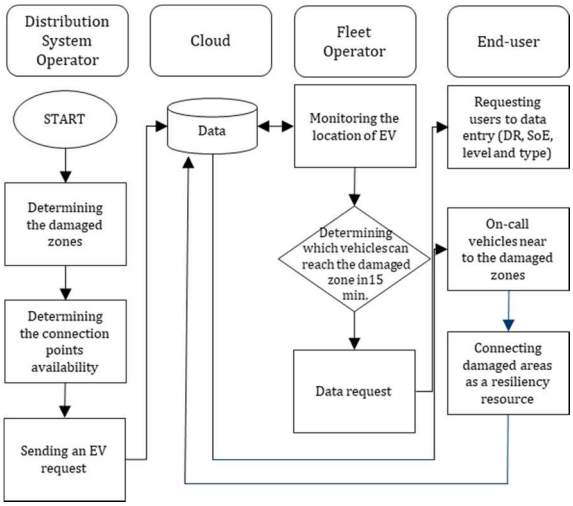

Fig. 5. Flow chart of the overall scheme consisting of multi-parties.

Besides, the operator can check the status of a specific bus by monitoring the number of connected vehicles, daily load curve in percentage, directed EVs as well as total restored demand after the optimal decision-making algorithm in the other tab. In this tab, the types and technical features of dispatched EVs can also be monitored by the operator.

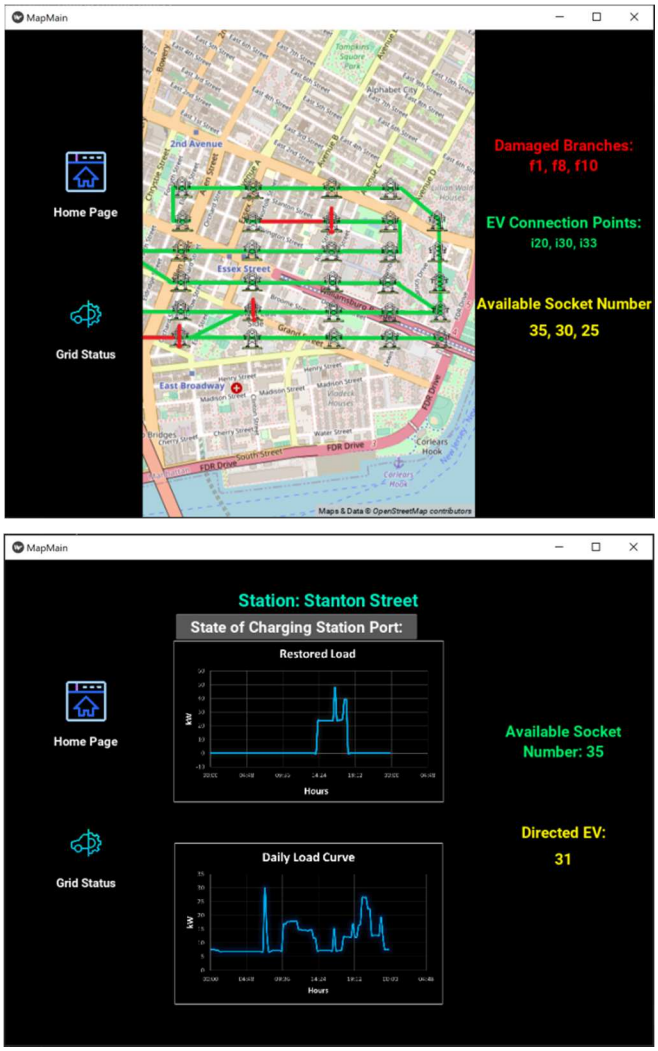

Fig. 6. The developed interface for distribution system operator (a) first tab and (b) second tab.

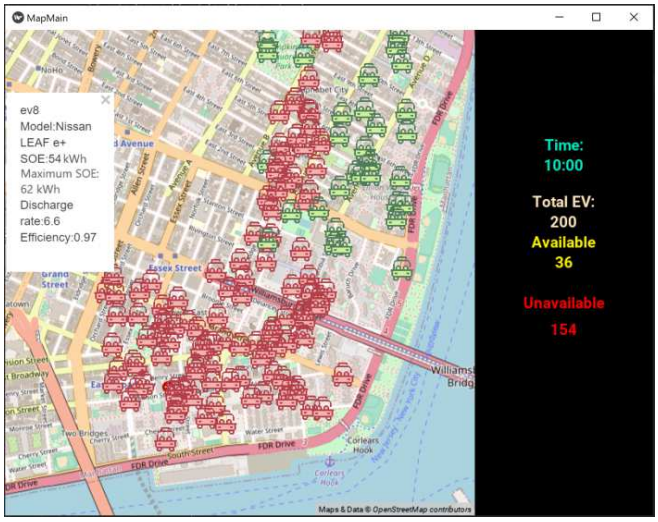

Fig. 7. The developed interface for fleet operator.

This article has been accepted for publication in a future issue of this journal, but has not been fully edited. Content may change prior to final publication. Citation information: DOI 10.1109/TSG.2022.3155438, IEEE Transactions on Smart Grid

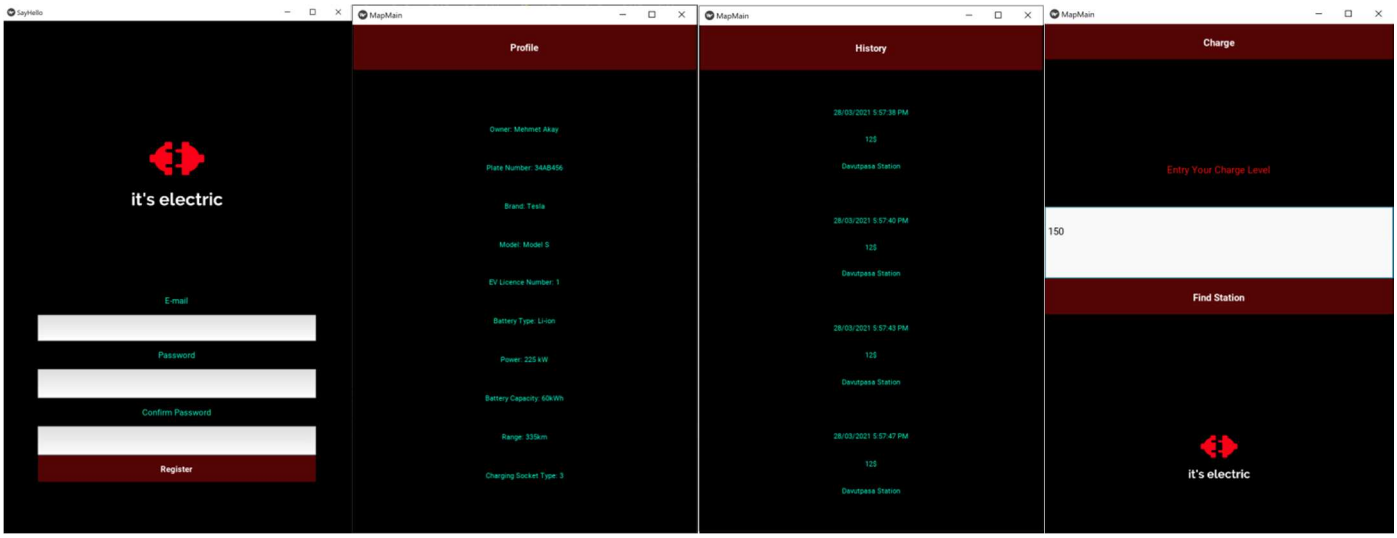

Fig. 8. EV user interfaces with the tabs of register, profile information, historical data, entering information.

Fig. 7 presents the fleet operator interface developed in the web-based platform in Google COLAB and then converted to a mobile application via Python Kivy framework. On the main page, the fleet operator can monitor the EVs within the ecosystem on a map. Also, it is possible to observe the technical specifications of the EVs and the locations thanks to bi-directional information exchange between parties. After, the arrival time of EVs from their current location to the damaged zones is calculated. EVs that can dispatch to the related area within 15 minutes or before are marked in green and those that will exceed 15 minutes are marked in red. Accordingly, the operator can determine available and non-available EVs in the other tab. Optimal dispatch plan depending on availability ma1trice is performed to increase system resiliency integrating on-call EV services. Information flow is carried out via mobile applications as stated in the previous section considering the potential hazards in communication infrastructure due to an event.

On the other hand, a mobile application for EV users enabling them to receive grid support requests from the fleet operator based on their location and technical specifications is a built-in Kivy Python framework. The developed interfaces depicted in Fig. 8 make it possible to respond to the invitation of becoming a resiliency resource in an emergency in one of the simplest yet most effective ways. For having permission to use the mobile application, EV users should be affiliated with the platform as an initial step and then become a member of the ecosystem. As it can be seen from the interfaces that EV users in the fleet convey the current/maximum/minimum SOE levels and maximum discharging rate of the vehicle with the data entry option.

The prepared interface enables it to receive and respond to signals through mobile internet. According to the data gathered from the distribution system operator containing the status of the power grid, the best possible EVs are directed from their service area to the damaged zones. EVs receive incentives due to becoming a participant for boosting resiliency. A contractual program is mandatory, i.e., it is strongly known that participants will face penalties in case they fail to receive a negative response. Feedbacks from the users are transmitted quickly to the interface for informing the operator.

Accordingly, an optimal decision-making algorithm is performed via integrating the input parameters into the scheme. On the other hand, the member can also view his/her history containing participation programs from the past. It is to highlight that the navigation subpart is not considered within the proposed concept; however, it could be developed with the aid of Google Maps API to manage emergency on-call EV services.

III. Mathematical Background of the Resiliency-Driven Strategy

A. Objective Function

In the objective function, the first term is the total served demand considering priority of the loads during simulation period. The second term is added for minimizing total losses in the branches. Since there are various EVs which have different specifications in the fleet, the third term is added to dispatch best possible vehicles for load restoration. Thus, it was aimed to optimize the decision-making process with dispatching minimum number of EV considering the available socket at the buses in order to avoid waste of resources.

The main aim of the propounded model is set to provide 100% restoration with optimally decreasing outage duration. On the other hand, redundant travels as well as losses due to causing extra costs are both targeted to reduce with determining appropriate weights. Assigning very small value to ε paved the way for evaluating second term insignificantly during simulation. In order to calculate objective function during whole simulation period in a stochastic manner, the related terms should be multiplied with equal probabilities of damaged location and event occurrence time scenarios (π_s, π_v).

Maximize

$$\sum_{s}\sum_{v}\pi_s \cdot \pi_v \left(\sum_{i}\sum_{d}\sum_{t}\left(w_d . u_{i,s,v,t}^{d}\right) - \varepsilon \cdot \sum_{l}\sum_{t} P_{l,s,v,t}^{loss} + \sum_{i}\sum_{e}\sum_{t}\beta_{i,e,s,v,t} \right) \quad (9)$$

B. Electric Vehicle Connection Constraints

Following an event, the fleet operator aims to dispatch best possible EVs to the damaged areas for serving critical loads.

However, any EV taking 1 in the availability matrix can participate in the resiliency enhancement strategy. Therefore, the decision variable ($\alpha_{i,e,s,v,t}$) can only be 1 if e vehicle is at a feasible zone in scenario s and v, as enforced in Eq. (10).

Available socket number is one of the most restrictive constraints while scheduling EVs in the connection points. Eq. (11) states that total number of directed EVs should be less than the capacity of related bus (κ_i). Constraint (12) is added to determine whether the EV is at transportation or connection phase. If the vehicle connects any available bus ($\alpha_{i,e,s,v,t} = 1$), then transportation variable ($\beta_{i,e,s,v,t}$) will get zero which is also used in objective function. Lastly, $\alpha_{i,e,s,v,t}$ should not take any value in the periods except arrival and departure periods as indicated in (13).

$$\alpha_{i,e,s,v,t} \le b_{i,e} \quad , \quad i \in i', \forall e \in E, \forall s, \forall v, t = t_{event} \tag{10}$$

$$\sum_{e} \alpha_{i,e,s,v,t} < \kappa_i \quad , \quad i \in i', t = t_{event} \tag{11}$$

$$\beta_{i,e,s,v,t} = 1 - \alpha_{i,e,s,v,t} \quad , \quad \forall i \in I, \forall e \in E, \forall t \in T, \forall s, \forall v \tag{12}$$

$$\alpha_{i,e,s,v,t} = 0 \quad , \quad \forall i \in I, \forall e \in E, \forall t \notin [t_{arrival}, t_{departure}] \tag{13}$$

C. Modelling of Electric Vehicles

Discharging power output of EV ($P^{dis}_{i,e,s,v,t}$) is determined based on multiplying with discharging rate of EV (DR_e obtained from specifications of battery) and connection variable ($\alpha_{i,e,s,v,t}$) for scenario s and v as stated in inequality (14). It will be zero while considering the periods except from arrival and departure times. In case of disruptive event, fleet operator makes a request for importing the information of SoE level of available EVs which are near the damaged zone. If candidate EV will participate in the load restoration strategy, $SOE_{i,e,s,v,t}$ is determined as initial SoE as indicated in Eq. (15). Travelling from staging locations to the damaged area causes loss of energy level (soe^{loss}_e) and therefore, SoE is calculated by subtracting loss energy from the current energy for more realistic assumptions as stated in (16). While EVs serve the critical loads, SoE variation is obtained proportional with the discharging power ($P^{dis}_{i,e,s,v,t-1}$) divided by battery efficiency (η_e) as well as multiplying with time granularity (ΔT) during the simulation period as represented in Eq. (17). For limiting the bound of minimum SoE level in order to avoid over-charging and deep-discharging, Inequality (18) is defined. Finally, discharging power output as well as SoE should be zero in the periods when EV is not plugged in any bus as denoted in (19).

$$P^{dis}_{i,e,s,v,t} \le \alpha_{i,e,s,v,t} . DR_e \, , \quad i \in i', \forall e \in E, \forall s, \forall v, t_{arrival} \le t < t_{departure} \tag{14}$$

$$SOE_{i,e,s,v,t} = soe_{e,t} . \alpha_{i,e,s,v,t}, \quad \forall i \in I, \forall e \in E, \forall s, \forall v, t = t_{event} \tag{15}$$

$$SOE_{i,e,s,v,t} = (soe_{e,t-1} - soe^{loss}_e) . \alpha_{i,e,s,v,t} \, , \quad \forall i \in I, \forall e \in E, \forall s, \forall v, t = t_{arrival} \tag{16}$$

$$SOE_{i,e,s,v,t} = SOE_{i,e,s,v,t-1} - \left(\frac{P^{dis}_{i,e,s,v,t-1}}{\eta_e}\right) . \Delta T \quad , \quad \forall i \in I, \forall e \in E, \forall s, \forall v, t_{arrival} < t \le t_{departure} \tag{17}$$

$$SOE_{i,e,s,v,t} \ge SOE_{min} . \alpha_{i,e,s,v,t} \quad , \quad \forall i \in I, \forall e \in E, \forall s, \forall v, t_{arrival} < t \le t_{departure} \tag{18}$$

$$SOE_{i,e,s,v,t} = 0, \quad P^{dis}_{i,e,s,v,t} = 0, \quad \forall i \in I, \forall e \in E, \forall t \notin [t_{arrival}, t_{departure}] \tag{19}$$

D. Mathematical Background of EV Motion

In order to calculate the remaining SoE that belongs to each EV when arriving the bus, the mathematical model of EV motion is considered in this paper. There are certain forces acting on an EV while it drives on the road. These forces are obtained on the basis of Newton's one-dimensional law of motion [29]. Eq. (20) expresses the sum of all forces acting on the vehicle. These forces represent the acceleration force ($\frac{dv(t)}{dt}$), aerodynamic force ($F_a(t)$), friction force ($F_r(t)$), gravitational force ($F_g(t)$), and other forces ($F_d(t)$), respectively. A detailed representation of the aforementioned forces is available in Eqs. (21)-(23). The value of $\frac{dv(t)}{dt}$ is obtained by dividing the difference of speeds in two consecutive seconds by the time interval in seconds (ΔT) as indicated in (24). EV consumes power while moving on the road and its value can be calculated by (25). Eq. (26) stated the mechanical power multiplying all forces acting on the vehicle by the speed in the relevant period. Finally, the mechanical power expression ($P_v(t)$) is divided by the driving efficiency (η_d) to calculate the power required for the movement of EV in period t. For more detailed explanations, Ref. [29] can also be examined.

$$F_t(t) = m_v . \frac{dv(t)}{dt} + F_a(t) + F_r(t) + F_g(t) + F_d(t) \tag{20}$$

$$F_a(t) = \frac{1}{2} . \rho . A . C_x . v(t)^2 \tag{21}$$

$$F_r(t) = m_v . C_r . g . \cos(\alpha) \tag{22}$$

$$F_g(t) = m_v . g . \sin(\alpha) \tag{23}$$

$$\frac{dv(t)}{dt} = \frac{v(t) - v(t-1)}{\Delta T} \tag{24}$$

$$P_v(t) = v(t) . F_t(t) \tag{25}$$

$$P(t) = \frac{P_v(t)}{\eta_d} \tag{26}$$

E. Power Flow Equations

Equation (27) states the general power balance formulation for all buses consisting of procured power from the substation bus ($P^{f,load}_{i,s,v,t}$), demanded power need of the bus ($P^{demand}_{i,s,v,t}$), actual power provided by EV discharging in the fleet ($P^{fleet}_{i,s,v,t}$) and the flowing power in the branches ($f_{l,s,v,t}$). Total discharging power of connected EVs to the candidate buses is equal to fleet output power as defined in (28).

Different types of critical loads (e.g., 1^{st}, 2^{nd}, 3^{rd} level) and non-critical load can exist at any bus in the distribution system. However, which of these loads can be supplied by EVs is determined according to the optimal decision-making algorithm.

Eq. (29) calculates to total restored demand of bus i ($P_{i,s,v,t}^{demand}$) based on rated power demand of d type load ($\delta_{d,t}$) multiplying with binary parameter ($h_{i,d}$) and variable ($u_{i,s,v,t}^{d}$). Related binary variable can take 1 if and only if the bus has related load type as defined in (30).

Also, flowing power limitation is described by the Eq. (31) describing that power flow ($f_{l,s,v,t}$) should be less than the maximum line capacity (f_l^{max}). On the other hand, the load demand of buses in scenario s and v ($P_{i,s,v,t}^{f,load}$) as well as total power losses ($\sum_{l\epsilon L} P_{l,s,v,t}^{loss}$) should be covered by the upstream grid ($P_{i,s,v,t}^{f}$) as stated in (32). Lastly, Eq. (33) enforces the fact that a range of injected power from upstream grid ($P_{i,s,v,t}^{f}$) cannot exceed the specified constraint ($P_i^{f,max}$) for reliable operation.

$$P_{i,s,v,t}^{f,load} + P_{i,s,v,t}^{fleet} + \sum_{\forall l\epsilon L: i\in\Omega_l^j} f_{l,s,v,t} - \sum_{\forall l\epsilon L: i\epsilon\Omega_l^i} f_{l,s,v,t} = P_{i,s,v,t}^{demand}, \quad \forall i \in I, \forall t \in T, \forall s, \forall v \tag{27}$$

$$P_{i,s,v,t}^{fleet} = \sum_{e} P_{i,e,s,v,t}^{dis}, \quad \forall i \in I, \forall t \in T, \forall s, \forall v \tag{28}$$

$$P_{i,s,v,t}^{demand} = \sum_{d} u_{i,s,v,t}^{d}.\delta_{d,t}.h_{i,d}, \quad \forall i \in I, \forall t \in T, \forall s, \forall v \tag{29}$$

$$u_{i,s,v,t}^{d} \le h_{i,d}, \quad \forall i \in I, \forall t \in T, d \in D, \forall s, \forall v \tag{30}$$

$$0 \le f_{l,s,v,t} \le f_l^{max}, \quad \forall l \in L, \forall t \in T, \forall s, \forall v \tag{31}$$

$$P_{i,s,v,t}^{f} = P_{i,s,v,t}^{f,load} + \sum_{l\in L} P_{l,s,v,t}^{loss}, \forall i \in \Omega_i^f, \forall t \in T, \forall s, \forall v \tag{32}$$

$$0 \le P_{i,s,v,t}^{f} \le P_i^{f,max}, \quad \forall i \in \Omega_i^f, \forall t \in T, \forall s, \forall v \tag{33}$$

F. Linearization of Power Losses

Power losses on a branch ($P_{l,s,v,t}^{loss}$) which is approximated using a quadratic function of power flow multiplying with the coefficients b and c is denoted in Eq. (34).

It is evidently clear that this statement cannot be used in MILP-based formulation due to its non-linear characteristics. Thus, Special Order Sets of Type 2 (SOS2) method is considered in linearization process and appropriate functions are obtained. SOS2 variables ($z_{l,s,v,t,p}$) in which most two adjacent elements can be non-zero are created for every branch, in scenarios s and v as represented in (35).

Afterwards, second-order function and power flow are approximated by using generated independent variables and constraints as indicated in Eqs. (36)-(37).

$$P_{l,s,v,t}^{loss} = b \cdot |f_{l,s,v,t}| + c \cdot {f_{l,s,v,t}}^2, \quad \forall l \in L, \forall t \in T \tag{34}$$

$$\sum_{p\in P} z_{l,s,v,t,p} = 1, \quad \forall l \in L, \forall t \in T \tag{35}$$

$$f_{l,s,v,t} = \sum_{p\in P} X_p.z_{l,s,v,t,p}, \quad \forall l \in L, \forall t \in T \tag{36}$$

$$F_{l,s,v,t} = \sum_{p\in P} Y_p.z_{l,s,v,t,p}, \quad \forall l \in L, \forall t \in T \tag{37}$$

IV. Numerical Results and Discussion

A. Input Data

The MILP-based mathematical formulation is simulated in the PuLP 1.6.8 open-source library of the Python 2.7 version using the CPLEX solver. A time granularity of 15 min is used in all numerical results and total time period is considered as 24 h.

The learning analyses and second step restoration model have been carried out on a personal computer with Intel Core I9, 3.60-GHz with 128 GB of RAM. The load profiles have been divided into 1^{st}, 2^{nd} and 3^{rd} level critical loads and non-critical loads based on data imported from [30]-[32]. It is assumed that there are four different types of EVs, i.e., Kia e-Soul, Hyundai Kona Electric, Nissan LEAF e+ and Opel Ampera-e, in the fleet and their detailed technical specifications can be found in [33].

B. Simulation Results

In order to illustrate the capabilities of the proposed optimal EV routing algorithm for maximizing power system resiliency, it is validated on IEEE-33 bus test feeder. Some of the branches are assumed to be damaged during an event and the loads after these branches cannot be supplied by the upstream grid.

1) Step 1: Forecasting Number of Available EVs

The overall yearly data are integrated into the system for two boroughs in Manhattan. Fig. 9 shows the univariate time series data of Two Bridges/Seward Park and trend, holidays, weekly and daily seasonality graphs are depicted in Figs. 10-13, respectively. Fig. 10 shows the trend of the dataset including upwards and downwards shift over time. According to the results, it is worthy to note that the number of yellow taxis usually shows a downward trend in December. Also, there is a sharp drop in the number of yellow taxis from April to September. Thanks to the trend illustration, underlying pattern of time series can be extracted.

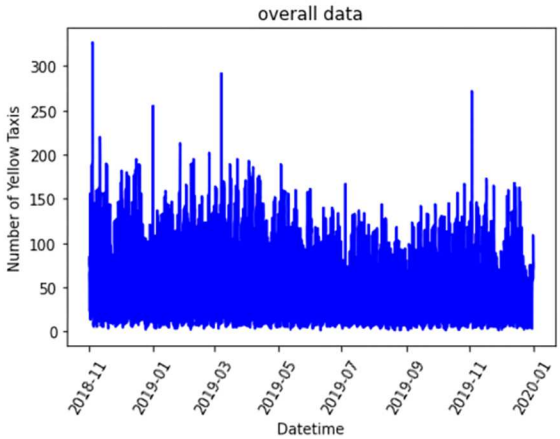

Fig. 9. Overall yearly data for Two Bridges/Seward Park in Manhattan.

This article has been accepted for publication in a future issue of this journal, but has not been fully edited. Content may change prior to final publication. Citation information: DOI 10.1109/TSG.2022.3155438, IEEE Transactions on Smart Grid

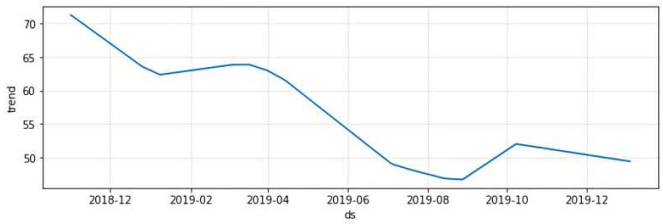

Fig. 10. Trend results for Two Bridges/Seward Park in Manhattan.

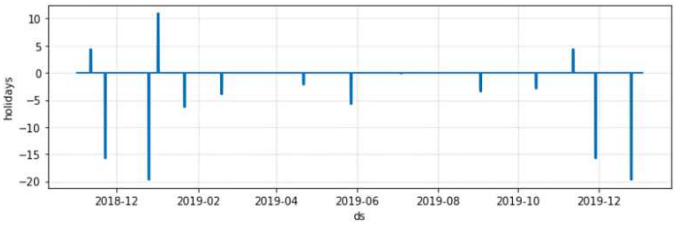

Fig. 11. Holidays' impacts on taxis number for Two Bridges/Seward Park in Manhattan.

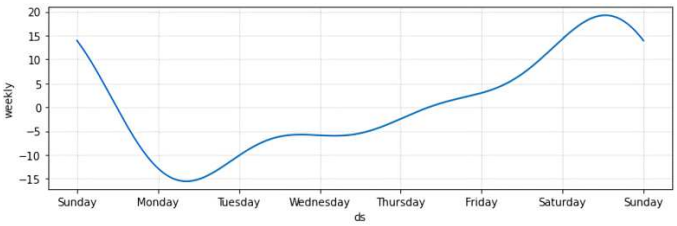

Fig. 12. Weekly seasonality on yellow taxis number for Two Bridges/Seward Park in Manhattan.

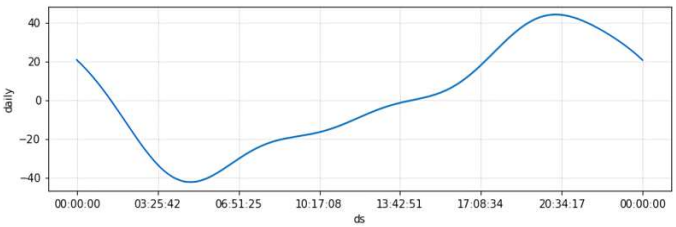

Fig. 13. Daily seasonality on yellow taxis number for Two Bridges/Seward Park in Manhattan.

The impact of holidays is also investigated for providing more accurate forecasting tool. New Year, Independence Day, Washington's Birthday and Labor Day are one of the considered holidays in learning-based analyses. It is seen that holidays have negative effect on the population of taxis.

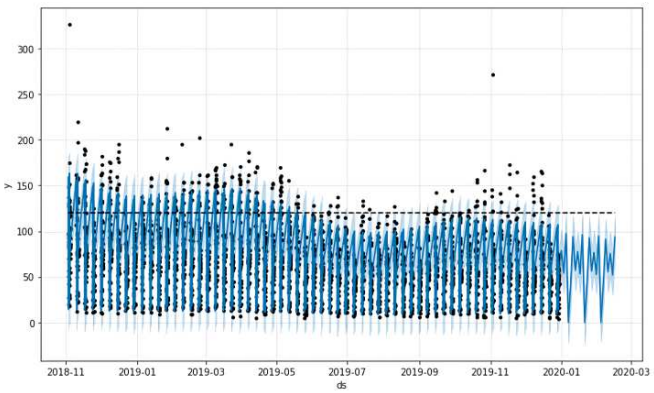

Fig. 14. Weekend prediction results for Two Bridges/Seward Park.

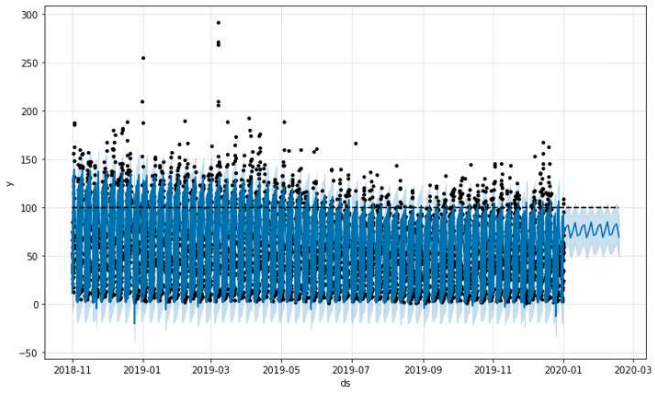

Fig. 15. Weekday prediction results for Two Bridges/Seward Park.

TABLE I
COMPARISON OF FORECAST RESULTS OBTAINED FROM DIFFERENT METHODOLOGIES

	MSE	RMSE	MAE	MAPE
PROPHET	216.93	14.72	10.96	0.199
Linear Regression	287.78	16.96	12.43	0.278
ARMA	256.31	16.00	13.49	0.443

Furthermore, the weekend and weekday data are considered, separately. The population of taxis on weekends is higher than weekdays. From Sunday to Monday, it shows a downward trend while upward trend is seen after that time. Furthermore, it tends to increase from 5am to 8pm during a day and it is decreasing after midnight.

Figs. 14-15 demonstrate the weekends and weekdays predictions by PROPHET for Two Bridges/Seward Park, respectively. The black points in the figures are the actual yellow taxis data and the blue line is the prediction curve of taxi population in related zone. One year data is used in training group and last 90 days are predicted. In these graphs, "ds" indicate the related date-time while "y" shows the number of yellow taxis.

In this study, linear regression and Autoregressive Moving Average (ARMA) models are used as benchmark for evaluating the performance of Facebook Prophet Algorithm based on out-of-sample forecast procedure using error measurements. Forecasted values are compared with actual data and standard indices which are mean squared error (MSE), root mean square error (RMSE), mean absolute error (MAE) and mean absolute percentage error (MAPE) are measured as indicated in Table I.

It is worth underlying that the RMSE and MAE values are quite high for all three models due to predicted number of yellow taxis. If the model is dealing with big numbers in dataset, then these RMSE and MAE prone to become bigger. On the contrary, small numbers pave the way for obtaining these mentioned indices as small. Since the yearly, monthly and daily seasonality as well as holidays are considered in Prophet Algorithm, it gave better results against to linear regression and ARMA.

In order to normalize and make it less impacted by whether the actual data is big or small, MAPE is used in this situation. The smaller MAPE indicates that forecast methodology gives better results. Therefore, it can be indicated that Prophet algorithm is advantageous compared to other techniques in forecasting the number of vehicles.

This article has been accepted for publication in a future issue of this journal, but has not been fully edited. Content may change prior to final publication. Citation information: DOI 10.1109/TSG.2022.3155438, IEEE Transactions on Smart Grid

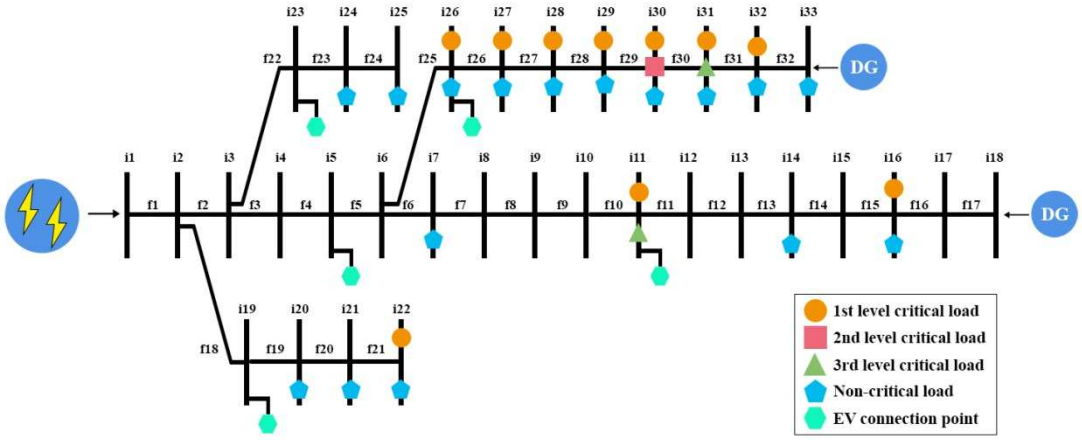

Fig. 16. The modified version of the IEEE-33 bus test feeder [34].

1) Step 2: Critical Load Restoration During Emergency Conditions

The number of available sockets is the main constraint of the proposed scheme that can certainly affect the number of EVs used in on-call service. The great amount of load curtailment can be prevented if and only if adequate number of sockets is available for directing EVs to the system. 1^{st} level critical loads are firstly supplied in the feeder and after the other loads at following feeders in radial distribution system when the line is damaged due to a HILP event. After, 2^{nd} and 3^{rd} level loads are fed sequentially, and non-critical loads can also be supplied if discharging power of arrived EVs is enough.

To investigate the capability of the developed stochastic programming-based algorithm, it is applied to the modified version of the IEEE-33 bus radial distribution system [34] as demonstrated in Fig. 16. Rated voltage of the related architecture is 12.66 kV. Loads with different priorities are randomly located into the buses. The main assumption is that the buses i_5, i_{11}, i_{19}, i_{23} and i_{26} have EV connection points including 15, 25, 10, 25 and 35 available sockets, respectively.

The supplemental resources are dispatched in the distribution system an immediate fashion after receiving signal from fleet operator from two staging places. These places can accommodate 150 and 200 EVs in their normal routine, respectively. As can be seen in Fig. 17, the test system is divided into three different seismic zones. The degree of ground shaking in the studied area during an extreme shock is quantified by the applied global AR model proposed in [18]. The generated AR equation based on multiple regression analysis is expressed in (38) as a function of hypo-central distance in rock site and moment magnitude.

$$\log(PGA) = 0.3646 + 0.4215M - 0.0187M^2 - 0.9707\log(R) - 0.0008(R) \quad (38)$$

It is to be highlighted that the presented model can be implemented in any region of the world which helps to perform seismic hazard analysis especially if an earthquake catalog is not available for that region. The vulnerability level of overhead distribution line sections due to a direct effect of an earthquake is mainly diagnosed with creating a high number of scenarios i.e., 100,000 for predefined each zona by MCS technique.

It is assumed that maximum hypocenter distance intervals for Zone #1, Zone #2, and Zone #3 are $220\ km < R_1 < 230\ km$, $200\ km < R_2 < 220\ km$ and $170\ km < R_3 < 200\ km$, respectively. On the other hand, the earthquake magnitude is specified between 6.0 to 6.5 for all generated scenarios via the MCS engine. Accordingly, 100,000 potential PGA for only Zone #1 is graphically illustrated in Fig. 18 due to page limitation. Besides, the status of branches following a seismic shock in terms of vulnerability is quantified and indicated in Table II. In this subsection, we take into consideration the damaged location and event occurrence time as a scenario-based stochastic approach based on probability theory declares whether an event occurred or not [35]. Stochastic modeling is a widely used method and it is very effective in capturing the dynamic characteristics of uncertainties. In the existing literature, probability density function or equal probability are utilized during the simulation of the model. According to the obtained results, scenarios are created considering the unavailability conditions of branches. The most important parameter while identifying the damaged location is to diagnose the fragility level of line sections.

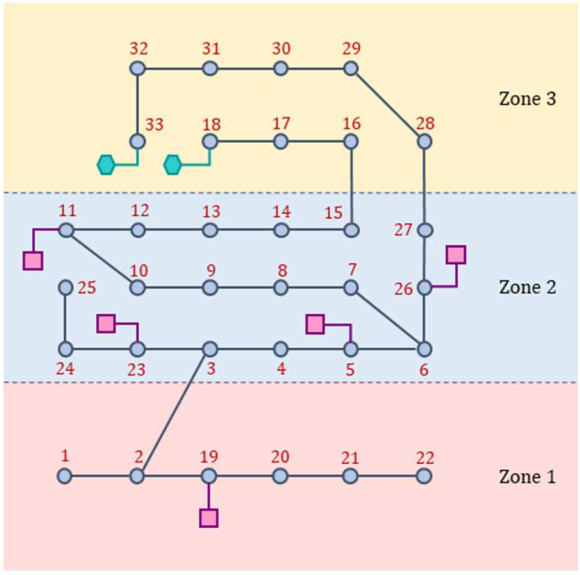

Fig. 17. IEEE-33 bus test system divided into seismic zones.

This article has been accepted for publication in a future issue of this journal, but has not been fully edited. Content may change prior to final publication. Citation information: DOI 10.1109/TSG.2022.3155438, IEEE Transactions on Smart Grid

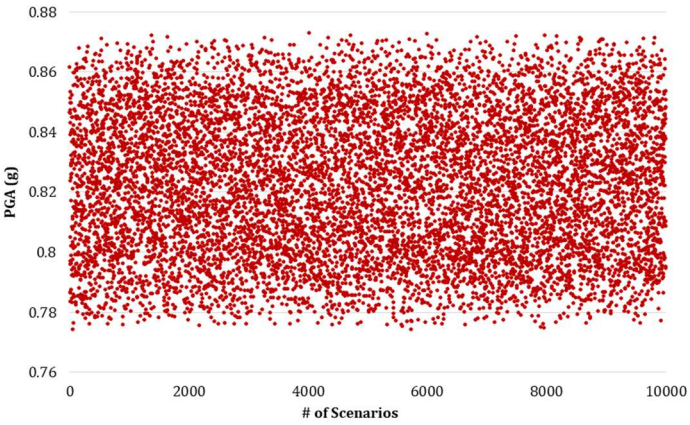

Fig. 18. Generated scenarios for PGA estimation in Zone 1.

TABLE II
UNAVAILABILITY OF DISTRIBUTION BRANCHES DUE TO SEISMIC SHOCK

Branch	v_n^{ls}	Branch	v_n^{ls}	Branch	v_n^{ls}
f_1	0.01432	f_{12}	0.01496	f_{23}	0.01330
f_2	0.01289	f_{13}	0.03325	f_{24}	0.02161
f_3	0.01995	f_{14}	0.02826	f_{25}	0.03325
f_4	0.00831	f_{15}	0.00665	f_{26}	0.02161
f_5	0.02161	f_{16}	0.01995	f_{27}	0.01829
f_6	0.03159	f_{17}	0.01496	f_{28}	0.01164
f_7	0.01164	f_{18}	0.02660	f_{29}	0.01995
f_8	0.02826	f_{19}	0.01575	f_{30}	0.03325
f_9	0.01662	f_{20}	0.01003	f_{31}	0.02992
f_{10}	0.01330	f_{21}	0.01575	f_{32}	0.01662
f_{11}	0.02660	f_{22}	0.02435		

Four different scenarios for damaged location and event occurrence time are considered to address the uncertainties caused by the seismic event as stated in Table III. It should be underlined that most risky branches which present low accessibility following an earthquake based on the abovementioned calculations are selected in this manner.

After combining the damaged location (called as $s_1 - s_4$) and event occurrence time scenarios (called as $v_1 - v_4$), 16 different scenarios are obtained in order to get accurate results which reflect the stochastic programming nature of the system as shown in Table IV. Scenario numbers and selection of the representative scenario are a substantial issue in a stochastic programming context. It should be reminded that the proposed methodology is appropriate for applying the desired number of scenarios. The load restoration in percentage for Scenario 1 to 8 and Scenario 9 to 16 is graphically represented in Fig. 19 (a) and (b), respectively. For the first scenario, load restoration reduces from 100% to 45.92% at 10:00 as can be deduced from the related figure. Although a great portion of the distribution system becomes unavailable at this period, load restoration rate did not decrease dramatically due primarily to integrated diesel generators at i_{33} and i_{18}. Similarly, it reaches its minimum value at 14:00, 18:00, and 22:00 for Scenarios 2 to 4 sequentially.

On the other hand, 79.13% of the load demand cannot be supplied by any source (e.g., upstream grid, EV, or diesel generator) in Scenario 5 to 8 following a seismic shock. However, the system performance starts to be improved thanks to deploying restorative actions step by step and more than 80% of the demand location of interest can be served. It should be underlined that damages in the line sections continue, i.e., the clearing process is not completed by the crews.

TABLE III
SCENARIOS OF DAMAGED BRANCHES AND EVENT OCCURRENCE TIME

	s_1	s_2	s_3	s_4
Damaged branches	f_{25}, f_{30}, f_{13}	$f_{25}, f_{30}, f_{31}, f_6, f_{13},$	f_{22}, f_8, f_{14}	f_{18}, f_{11}
	v_1	v_2	v_3	v_4
Event occurrence time	10:00	14:00	18:00	22:00
Duration [h]	4	4	4	1,75

TABLE IV
CREATED SCENARIOS FOR CASE STUDIES

Time↓ /Location→	s_1	s_2	s_3	s_4
v_1	Scenario 1	Scenario 5	Scenario 9	Scenario 13
v_2	Scenario 2	Scenario 6	Scenario 10	Scenario 14
v_3	Scenario 3	Scenario 7	Scenario 11	Scenario 15
v_4	Scenario 4	Scenario 8	Scenario 12	Scenario 16

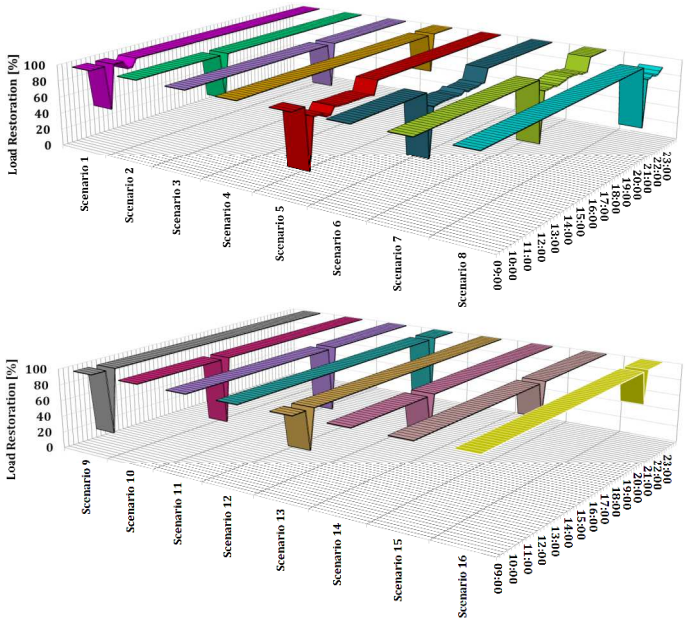

Fig. 19. Load restoration results for all scenarios (a) from Scenario 1 to 8 during simulation (b) from Scenario 9 to 16 during simulation.

Before a critical HILP disturbance, the power system can be operated in reliable fashion. Namely, injected power from the upstream grid could meet the complete system demand. After an event occurrence time, load restoration is boosted substantially by exploiting the remarkable potential of V2G which offers an improved power system resiliency. It is seen that 100% of the demand is fully satisfied for Scenarios 9-16 during a simulation except for the period of the event.

Fig. 20 presents the output power of diesel generators placed at i_{33} and i_{18} for Scenario 1 to 4 and their contribution to supplying the demand in formed islands. Since the amount of load requirement to be served by the generator connected to the i_{33} is relatively higher than the i_{18}, the distinct difference occurs between the provided power of the integrated sources as can be deduced from the figure. It reaches its peak value for v_3 depending strongly on the power demand of buses in the islanded area. The most significant conclusion to be extracted from this analysis is that diesel generators also help to increase power system resiliency, especially during an emergency condition when encountered with unintentional islanding.

This article has been accepted for publication in a future issue of this journal, but has not been fully edited. Content may change prior to final publication. Citation information: DOI 10.1109/TSG.2022.3155438, IEEE Transactions on Smart Grid

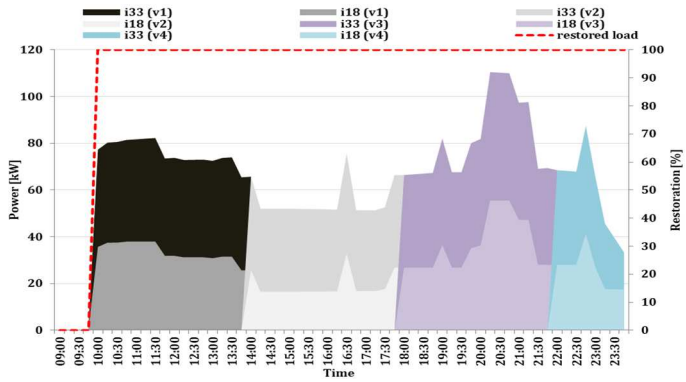

Fig. 20. The output power of diesel generators for Scenario 1 to 4 with load restoration rate.

The fleet output power on buses that have connection points for several scenarios is graphically demonstrated in Fig. 21. In Scenario 1, demanded power of the i_{26} and subsequent buses is met by 31 EVs while after a period of the HILP disturbance for boosting survivability of the critical loads. Although a high number of on-call services are connected to the stations, the load restoration did not reach the 100% level due mainly to the available socket number. It is changing from 45.92% to 90.07%, i.e., the load of i_{29} and i_{30} buses are not matched by V2G option in some periods. The non-critical loads at mentioned buses are not satisfied which has lowest priority coefficients and no more vehicles are called just meet these load demand as expected. 4^{th} level critical loads placed at i_{29} and i_{30} reach their maximum value from 10:00 to 14:00, and therefore procured power from on-call services is not becoming enough.

On the other hand, full load restoration thanks to managing EV fleets is performed for Scenarios 9 to 16 due to the relatively low power demand of damaged zones. Discharging power output is matched by demanded power of i_{11} and i_{23} and as well as their subsequent buses. The power balance of bus i_{26} including served demand of consecutive buses (i.e., i_{26} to i_{33}), power losses occurred in the branches from f_{26} up to f_{32}, the provided power from the diesel generator and as well as total energy resource (means total SoE level of directed on-call EV services at the beginning of the scenario) and discharging power during emergency condition is illustrated in Fig. 22.

The upstream grid is capable of supplying the demanded power of the loads without interruption in pre-event and post-event timeframes. However, there occurs a disruption at 10:00 for the scenario of interest and supplementary resources are activated concerning resiliency enhancement strategies.

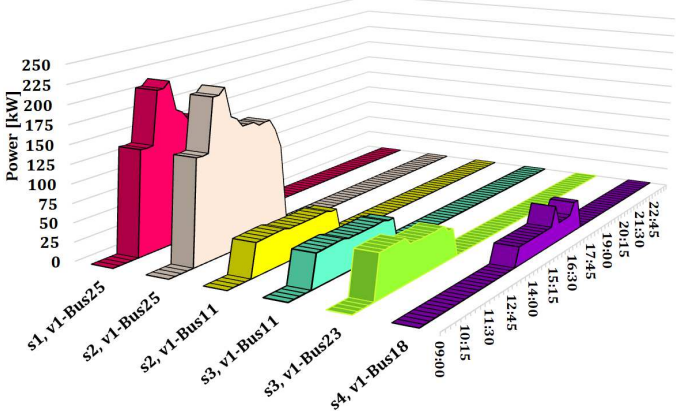

Fig. 21. Fleet discharging results for buses for Scenarios 1, 5, 9, 13.

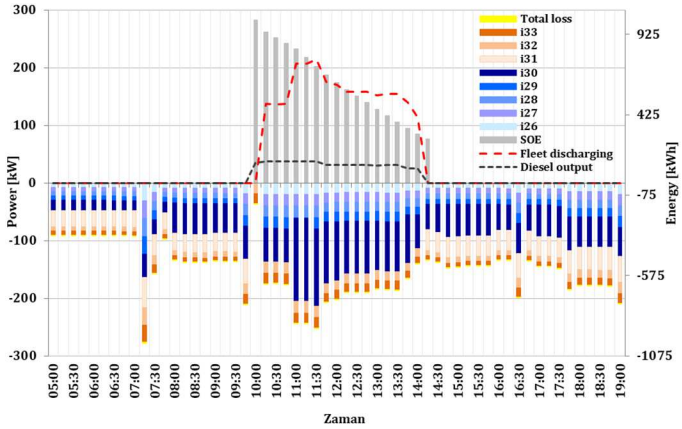

Fig. 22. The power balance of bus i_{26} for Scenario 5.

At 10:00, a great portion of loads in the formed island experiences a power outage from the main grid except i_{32} and i_{33} as can be deduced from the related figure. They are supplied by the diesel generator until clearing the damaged in line sections f_{30} and f_{31}. When the specific time of the day such as from 10:00 to 14:00 is examined in detail, it is observed that on-call EV service output is aligning with the total demand of related buses and as well as power losses in the branches.

On the other hand, available SoE capacity tends to reduce due primarily to this dynamic component's discharging periods determined by the proposed optimal decision-making algorithm. The comprehensive results show that the optimization-based strategy performs properly as expected, indicating the accuracy of the presented scheme. Also, the dynamic characteristics of load pattern and uncertain nature of HILP event can be captured thanks to conducting stochastic-based model with respect to resiliency concept. Managing mobile and static emergency resources contributes to increasing system performance as indicated in obtained optimal results.

The variation of the injected power from the upstream grid is demonstrated in Fig. 23 to simplify the interpretation of the results for the considered 16 scenarios. Box-whiskers are commonly used in the literature so as to show the distribution of the data set. The line in the middle of the boxes states the median of the drawn power for all scenarios of interest during simulation. The median divides the data into two parts namely, first and third quartiles. Lastly, whiskers show the maximum and minimum power values with the end of the vertical lines.

As an example, the transferred power varies between 88.26 kW to 473.145 kW; 25% of the data is greater than 473.145 kW while 25% of the data is lower than 398. 583 kW at 11:00 considering all possibilities.

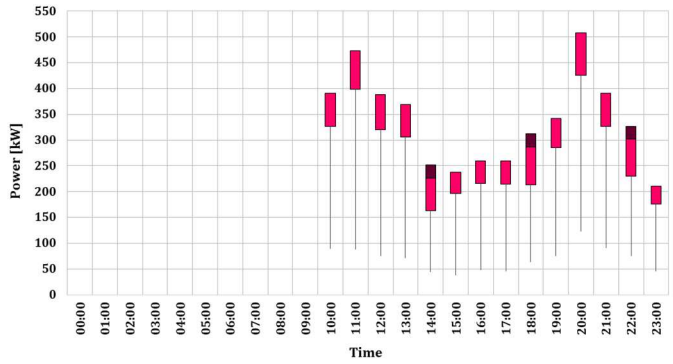

Fig. 23. The variations of the drawn power from the upstream grid for all scenarios.

Since any disruption is not the issue until 10:00, the amount of drawn power for all scenarios is the same at the corresponding time of the day as can be seen in the related graph. From the other perspective, the deviation in procured power for considered scenarios becomes evident at 20:00. The differences between maximum and minimum values of transferred power become clear especially for the scenarios considering v_1 and v_2. The reason for high deviations can be explained that the highest load demand of the distribution system (from i_{26} to i_{33}) is fully curtailed in some scenarios and this enables to reach supplied power at the minimum point.

Table V encapsulates the 16 scenarios assessed in this study by considering the unavailability of overhead distribution branches following a seismic event. According to the results, load restoration of damaged locations becomes 93.13% in Scenario 1, and it is evident that if such a scheme was not implemented, the loss of load rate would be very high. On-call EV services operate in V2G mode for matching the 1074.840 kWh demand of critical loads with high priority.

On the other hand, relatively load restoration after an interruption emerges in Scenarios 5 to 8 when comparing the other considered scenarios. The main reason behind this is that the highest demanded power cannot be fully matched either diesel generator or EV services due to the inaccessibility of the f_{31} branch. Since the demanded load is met by 100% except the beginning of the event, the restoration rate has reached more than 92% for Scenarios 13 to 15.From the results, it can be seen that the proposed scheme has an efficient performance in terms of boosting power system resiliency.

Note that, obtaining approximately 95% restoration does not only show superiority of using scenario-based stochastic approach, but also indicates that this value can be even increased considering a larger distribution system integrating with more emergency resources. Besides, 16 potential scenarios enable to obtain more realistic system scheduling. Moreover, the decisions are more accurate and closer to what can be realistically expected in practical implementations. If this kind of framework had not been presented, total loss of load would have been 100% and all critical loads would have been curtailed in low resilient power system.

TABLE V
RESULTS OF THE EVALUATED SCENARIOS STOCHASTIC BASED ANALYSES

	Probability	Total demand during an event [kWh]	Supplied energy by EVs [kWh]	Load restoration [%]
Scenario 1	0.097376	1154.065	1074.840	93.13
Scenario 2	0.288184	724.345	672.906	92.89
Scenario 3	0.079735	1045.080	994.112	95.12
Scenario 4	0.129586	341.898	294.362	86.09
Scenario 5	0.056531	1333.524	1074.840	80.60
Scenario 6	0.067179	878.878	672.906	76.56
Scenario 7	0.054959	1236.438	994.113	80.40
Scenario 8	0.050131	409.747	294.363	71.84
Scenario 9	0.028149	386.578	363.070	93.91
Scenario 10	0.034277	273.053	253.702	92.91
Scenario 11	0.025058	415.872	396.239	95.27
Scenario 12	0.032575	142.025	121.725	85.70
Scenario 13	0.009734	461.298	433.101	93.88
Scenario 14	0.006889	318.796	295.986	92.84
Scenario 15	0.019377	497.490	474.218	95.32
Scenario 16	0.020262	169.837	145.748	85.81

V. CONCLUSION AND FUTURE WORK

In this paper, a resiliency-driven multi-step critical load restoration strategy for distribution system integrating on-call EVs under fleet operator framework ahead an HILP event was proposed. The main objective of the presented model was to maximize the cumulated service time for loads, weighted by their priority, with the minimum number of EVs. In the first step, the random nature of the seismic event was handled by creating a high number of hazard scenarios via MCS method. Then, the failure probabilities of the overhead distribution branches after an extreme event were determined within the fragility curve concept. In the second step, the location and the number of EVs in the related zone were forecasted by performing learning-based analyses for capturing mobility-based uncertainties of EVs using the PROPHET algorithm, considering daily, weekly and yearly seasonality, as well as holiday effects. Finally, MILP-based optimal restoration plan was performed on IEEE-33-bus test feeders for clearly illustrating the capabilities of the model in the PuLP 1.6.8 open-source library of Python 2.7 version, solved by the CPLEX solver by using the obtained input parameters. The stochasticity regarding the damaged location and event occurrence time was taken into consideration in the scenario-based stochastic model for capturing the inherent uncertainties. Numerical results proved the effectiveness of the proposed framework. The outage scale and duration of critical and even non-critical loads after an event were reduced substantially due to the optimal dispatching of EVs. The load restoration was increased at least 71.84%, at most 95.32%, depending on the available socket number, available number of EVs, the event occurrence time and location. However, if the algorithm had not been implemented, it is clear that the total loss of load would have been 100% during an emergency condition and the distribution system would have been operated in a low resilient fashion. Furthermore, for facilitating the real-world implementation of such concepts, interfaces for three stakeholders were developed in the Python Kivy framework and presented in detail. Integrating the transportation system constraints into the proposed concept can be considered as a future direction.

VI. REFERENCES

[1] G. M. Karagiannis, S. Chondrogiannis, E. K. Zehra, and I. Turksezer, *Power grid recovery after natural hazard impact - a Science for Policy report*, no. December. 2017.

[2] E. B. Watson and A. H. Etemadi, "Modeling Electrical Grid Resilience under Hurricane Wind Conditions with Increased Solar and Wind Power Generation," *IEEE Trans. Power Syst.*, vol. 35, no. 2, pp. 929–937, 2020.

[3] Yuan, W., Jian, H.W., Feng, Q., et al.: 'Robust optimization-based resilient distribution network planning against natural disasters', *IEEE Trans. Smart Grid*, 2016, 7, (6), pp. 2817–2826

[4] W. Sun, N. Kadel, I. Alvarez-Fernandez, R. R. Nejad, and A. Golshani, "Optimal distribution system restoration using PHEVs," *IET Smart Grid*, vol. 2, no. 1, pp. 42–49, 2019.

[5] Y. Ma, T. Houghton, A. Cruden, and D. Infield, "Modeling the benefits of vehicle-to-grid technology to a power system," *IEEE Trans. Power Syst.*, vol. 27, no. 2, pp. 1012–1020, 2012.

[6] K. Rahimi and M. Davoudi, "Electric vehicles for improving resilience of distribution systems," *Sustain. Cities Soc.*, vol. 36.

[7] H. Mehrjerdi and R. Hemmati, "Coordination of vehicle-to-home and renewable capacity resources for energy management in resilience and self-healing building," *Renew. Energy*, vol. 146, pp. 568–579, 2020.

[8] H. Shin and R. Baldick, "Plug-In Electric Vehicle to Home (V2H) Operation under a Grid Outage," *IEEE Trans. Smart Grid*, vol. 8, no. 4, pp. 2032–2041, 2017.

[9] S. Lei, J. Wang, C. Chen, and Y. Hou, "Mobile Emergency Generator Pre-Positioning and Real-Time Allocation for Resilient Response to Natural Disasters," *IEEE Trans. Smart Grid*, vol. 9, no. 3, pp. 2030–2041, 2018.

[10] Z. Yang, P. Dehghanian, and M. Nazemi, "Seismic-Resilient Electric Power Distribution Systems: Harnessing the Mobility of Power Sources," *IEEE Trans. Ind. Appl*., vol. 56, no. 3, pp. 2304–2313, 2020.

[11] H. Gao, Y. Chen, S. Mei, S. Huang, and Y. Xu, "Resilience-Oriented Pre-Hurricane Resource Allocation in Distribution Systems Considering Electric Buses," *Proc. IEEE*, vol. 105, no. 7, pp. 1214–1233, 2017.

[12] Y. Xu, Y. Wang, J. He, M. Su, and P. Ni, "Resilience-Oriented Distribution System Restoration Considering Mobile Emergency Resource Dispatch in Transportation System," *IEEE Access*, vol. 7, pp. 73899–73912, 2019.

[13] S. Lei, C. Chen, Y. Li, and Y. Hou, "Resilient Disaster Recovery Logistics of Distribution Systems: Co-Optimize Service Restoration with Repair Crew and Mobile Power Source Dispatch," *IEEE Trans. Smart Grid*, vol. 10, no. 6, pp. 6187–6202, 2019.

[14] P. M. De Quevedo, J. Contreras, A. Mazza, G. Chicco, and R. Porumb, "Reliability Assessment of Microgrids With Local and Mobile Generation, Time-Dependent Profiles, and Intraday Reconfiguration," *IEEE Trans. Ind. Appl*., vol. 54, no. 1, pp. 61–72, 2018.

[15] J. Kim and Y. Dvorkin, "Enhancing Distribution System Resilience with Mobile Energy Storage and Microgrids," *IEEE Trans. Smart Grid*, vol. PP, no. c, p. 1, 2018.

[16] A. Gholami, T. Shekari, F. Aminifar, and M. Shahidehpour, "Microgrid Scheduling with Uncertainty: The Quest for Resilience," *IEEE Trans. Smart Grid*, vol. 7, no. 6, pp. 2849–2858, 2016.

[17] K. Balasubramaniam, P. Saraf, R. Hadidi, and E. B. Makram, "Energy management system for enhanced resiliency of microgrids during islanded operation," *Electr. Power Syst. Res*., vol. 137, pp. 133–141, 2016.

[18] A. Shiuly, "Global Attenuation Relationship for Estimating Peak Ground Acceleration," *J Geol Soc India*, vol. 92, no. 1, pp. 54–58, Jul. 2018, doi: 10.1007/s12594-018-0952-4.

[19] G. G. Amiri, A. Mahdavian, and F. M. Dana, "Attenuation Relationships for Iran," *Journal of Earthquake Engineering*, vol. 11, no. 4, pp. 469–492, Jul. 2007, doi: 10.1080/13632460601034049.

[20] M. Nazemi and P. Dehghanian, "Seismic-Resilient Bulk Power Grids: Hazard Characterization, Modeling, and Mitigation," *IEEE Transactions on Engineering Management*, vol. 67, no. 3, pp. 614–630, Aug. 2020, doi: 10.1109/TEM.2019.2950669.

[21] B. Li, R. Roche, and A. Miraoui, "A temporal-spatial natural disaster model for power system resilience improvement using DG and lines hardening," in *2017 IEEE Manchester PowerTech*, Jun. 2017, pp. 1–6. doi: 10.1109/PTC.2017.7980851.

[22] M. Ghasemi, A. Kazemi, R. Dashti, M. A. Rajabi, and M. A. Gilani, "Resilience Evaluation and Prediction in Electrical Distribution Systems: A Case Study in Golestan Province," in *EPDC 2019*, Jun. 2019, pp. 6–9. doi: 10.1109/EPDC.2019.8903863.

[23] H. Saboori, R. Hemmati, S. M. S. Ghiasi, and S. Dehghan, "Energy storage planning in electric power distribution networks – A state-of-the-art review," *Renewable and Sustainable Energy Reviews*, vol. 79, pp. 1108–1121, Nov. 2017, doi: 10.1016/j.rser.2017.05.171.

[24] U. S. F. E. M. A. http://www.fema.gov, "Multi-hazard Loss Estimation Methodology: Earthquake Model, Hazus-MH 2.1: User Manual," presented at the United States. Federal Emergency Management Agency, Jan. 1969. Accessed: Aug. 25, 2021. [Online]. Available: https://www.hsdl.org/?abstract&did=

[25] TLC Trip Record Data, NYC, May 20, 2020. [Online]. Available: https://www1.nyc.gov/site/tlc/about/tlc-trip-record-data.page.

[26] W. X. Fang, P. C. Lan, W. R. Lin, H. C. Chang, H. Y. Chang, and Y. H. Wang, "Combine Facebook Prophet and LSTM with BPNN Forecasting financial markets: The Morgan Taiwan Index," *Proc. - 2019 Int. Symp. Intell. Signal Process. Commun. Syst. ISPACS 2019*, pp. 0–1, 2019.

[27] G. Borowik, Z. M. Wawrzyniak, and P. Cichosz, "Time series analysis for crime forecasting," *26th Int. Conf. Syst. Eng. ICSEng 2018 - Proc*., 2019.

[28] F. Duvodq, V. W. X. Nkdv, H. G. X. Wu, and A. Dataset, "Bitcoin Forecasting using ARIMA and PROPHET" vol. C, pp. 6–9, 2016.

[29] Şengör, İ., Erenoğlu, A. K. , Erdinç, O., Taşcıkaraoğlu, A., & Catalao, J., (2020). Day-ahead charging operation of electric vehicles with on-site renewable energy resources in a mixed integer linear programming framework. *IET Smart Grid* , vol.1, 1.

[30] D. Niyato, X. Lu, and P. Wang, "Adaptive power management for wireless base stations in a smart grid environment," *IEEE Wirel. Commun*., vol. 19, no. 6, pp. 44–51, 2012.

[31] A. Ayang, P.-S. Ngohe-Ekam, B. Videme, and J. Temga, "Power Consumption: Base Stations of Telecommunication in Sahel Zone of Cameroon: Typology Based on the Power Consumption—Model and Energy Savings," *J. Energy*, vol. 2016, pp. 1–15, 2016.

[32] Hastane & Otel & Alışveriş Merkezi ve Üniversite Kampüslerinde Kojenerasyon Uygulamaları/Kapasite Seçiminde Optimizasyon, UCTEA Chamber of Mechanical Engineers, May 20, 2020. [Online] Available: https://www.mmo.org.tr/sites/default/files/gonderi_dosya_ekleri/72e4ff749ee6abb_ek_3.pdf.

[33] Electric Vehicles Database. May 20, 2020. [Online] Available: https://ev-database.org/

[34] M. Zadsar, M. R. Haghifam, and S. M. M. Larimi, "Approach for self-healing resilient operation of active distribution network with microgrid," *IET Gener. Transm. Distrib*., vol. 11, no. 18, pp. 4633–4643, 2017.

[35] A. Omishore and L. Puklický, "Fuzzy Probabilistic Models , Uncertainty and Structural Reliability," no. March, 2009.